

## Third-generation muffin–tin orbitals

O K ANDERSEN\*, T SAHA-DASGUPTA<sup>†</sup> and S EZHOV

Max-Planck Institut für Festkörperforschung, D-70569, Stuttgart, Germany

<sup>†</sup>S.N. Bose Centre, Kolkata 700 098, India

**Abstract.** By the example of  $sp^3$ -bonded semiconductors, we illustrate what 3rd-generation muffin–tin orbitals (MTOs) are. We demonstrate that they can be downfolded to smaller and smaller basis sets:  $sp^3d^{10}$ ,  $sp^3$ , and bond orbitals. For isolated bands, it is possible to generate Wannier functions *a priori*. Also for bands, which overlap other bands, Wannier-like MTOs can be generated *a priori*. Hence, MTOs have a unique capability for providing chemical understanding.

**Keywords.** Band structure; density functional; LMTO; Wannier functions.

### 1. Introduction

Muffin–tin orbitals (MTOs) have been used for a long time in *ab initio*, e.g. density-functional (DF) calculations of the electronic structure of condensed matter. Over the years, several MTO-based methods have been developed. The ultimate aim is to find a generally applicable electronic-structure method which is intelligible, fast, and accurate.

In order to be intelligible, an electronic-structure method must employ a minimal and flexible basis of short-ranged orbitals. As an example, the method should be able to describe the valence band and the lower part of the conduction band in  $sp^3$ -bonded materials using merely four short-ranged *s*- and *p*-orbitals per atom and, for insulating phases, using merely occupied orbitals such as bond orbitals. Another example is materials with strong electronic correlations. For such materials, one must first construct a small, but realistic Hilbert space of many-electron wave functions, and this requires an accurate and flexible single-particle basis of atom-centred short-ranged orbitals. A small basis of short-ranged orbitals is a prerequisite for a method to be intelligible and fast, but it may be a hindrance for its accuracy, because the orbitals of a smaller basis tend to be more complicated than those of a larger basis.

Most other density-functional methods, such as plane-wave pseudopotential, LAPW, PAW, and LCAO methods, aim at simulation, and are therefore primarily accurate and robust. But they are neither fast nor intelligible in the above-mentioned sense, because they employ basis sets with order of hundred functions per atom. With such methods, understanding can therefore only be attempted after the calculation, by means of projections onto e.g. Wannier functions in case of insulators, charge

densities, electron-localization functions (ELFs), partial waves, a.s.o.

The so-called 3rd-generation MTO method (Andersen *et al* 1994, 1998, 2000; Andersen and Saha-Dasgupta 2000; Tank and Arcangeli 2000) should come close to what we have been aiming for. In the present paper we shall explain what 3rd-generation MTOs are and what they achieve. Emphasis will be on the so-called down-folding and energy-mesh features which enable MTO bases to be small, flexible, and accurate, as we shall demonstrate by exposing them to the above-mentioned  $sp^3$ -test. From the result, the idea emerges, that for band insulators, an MTO basis can be designed *a priori* to span the Hilbert space of the occupied states only. That is, there is one, and only one, such MTO per electron. To get this count right, one may associate each orbital with a nominal electron (or pair), and leave it to the method to shape the orbitals in such a way that the basis set becomes complete for the occupied states. This can be done because MTOs are selective in energy, in the sense that the MTOs of order  $N$  (NMTOs) are shaped in such a way that the NMTO basis set solves Schrödinger's equation exactly for  $N+1$  single-particle energies, which in the present case must be chosen in such a way that they span the valence band. This ability to generate Wannier functions directly in real space, should be useful for *ab initio* molecular-dynamics simulations. NMTOs may also prove useful for designing many-electron wave functions, which describe correlated electron systems in a realistic way. The description of spin and orbital ordering is a trivial example. Also for the conduction bands of metals, Wannier-like, low-energy MTOs can be designed *a priori*. This has been demonstrated in several cases (Müller *et al* 1998; Korotin *et al* 2000; Sarma *et al* 2000; Valenti *et al* 2001; Dasgupta *et al*, to be published), most recently for the hole-doped cuprate high-temperature superconductors, where the material-dependent trend of the hopping integrals and their correlation with the maximum  $T_c$

\*Author for correspondence

was discovered (Pavarini *et al* 2001; Dasgupta *et al*, to be published).

For a description of how we expand the charge density locally in such a way that Poisson's equation can be solved and the total energy and forces can be evaluated fast and accurately, we refer to previous (Andersen *et al* 2000; Tank and Arcangeli 2000) and coming publications (Arcangeli and Andersen, Savrasov and Andersen). This part of the 3rd-generation computer code is still under construction.

## 2. Screened spherical waves, kinked partial waves and muffin-tin orbitals

The 3rd-generation MTO formalism is the multiple-scattering—or KKR (Korringa 1947; Kohn and Rostoker 1954)—formalism for finding the solutions,  $\mathbf{Y}_i(\mathbf{r})$ , of Schrödinger's equation for an electron in a muffin tin potential,  $V(\mathbf{r}) = \sum_R v_R(r_R)$ , with the following three extensions:

- (i) The KKR formalism is proved to hold, not only for superpositions of spherically-symmetric, non-overlapping potential wells,  $v_R(r_R)$ , but also to leading order in the potential-overlap (Andersen *et al* 1992). Here, and in the following,  $r_R \equiv |\mathbf{r} - \mathbf{R}|$ , and  $\mathbf{R}$  are the sites which we label by  $R$ . The potential,  $v_R(r)$ , is taken to vanish outside a radius,  $s_R$ , which should not exceed 1.6 times the radius of touching spheres, i.e.  $s_R + s_{R'} \lesssim 1.6|\mathbf{R} - \mathbf{R}'|$  for any pair of sites,  $R$  and  $R'$ .
- (ii) Exact screening transformations of the spherical waves,  $n_l(\mathbf{k}_R)Y_L(\hat{\mathbf{r}}_R)$ , are introduced in order to reduce the spatial range and the energy dependence ( $\mathbf{k} \equiv \mathbf{e}$ ) of the wave-equation solutions,  $\mathbf{y}_{RL}(\mathbf{e}, \mathbf{r})$  (Andersen and Jepsen 1984; Andersen *et al* 1992; Zeller *et al* 1995). Here, and in the following,  $L \equiv lm$  labels the spherical- (or cubic-) harmonic's character.
- (iii) Energy-independent MTO basis sets are derived which span the solutions  $\mathbf{y}_i(\mathbf{r})$  with energies,  $\mathbf{e}$ , of Schrödinger's equation to within errors proportional to  $(\mathbf{e} - \mathbf{e}_0)(\mathbf{e} - \mathbf{e}_1) \dots (\mathbf{e} - \mathbf{e}_N)$ , where  $\mathbf{e}_0, \mathbf{e}_1, \dots, \mathbf{e}_N$  is a chosen energy mesh with  $N+1$  points (Andersen *et al* 2000; Andersen and Saha-Dasgupta 2000). Such an energy-independent set of  $N$ th-order MTOs is called an NMTO set. By virtue of the variational principle, the errors of the energies  $\mathbf{e}$  will be proportional to  $(\mathbf{e} - \mathbf{e}_0)^2(\mathbf{e} - \mathbf{e}_1)^2 \dots (\mathbf{e} - \mathbf{e}_N)^2$ .

At the top of figure 1 we show the LDA energy bands,  $\mathbf{e}(\mathbf{k})$ , of Si in the diamond structure, calculated with the basis set of Si-centred  $s$ -,  $p$ -, and  $d$ -MTOs, i.e. with 9 orbitals/atom, for the 3-point energy mesh  $\mathbf{e}_0, \mathbf{e}_1, \mathbf{e}_2$  indicated on the right-hand side. These bands have meV-

accuracy for the MT-potential, which in the present case was the standard all-electron DF-LDA atomic-spheres potential. Since three energy points were used, the MTOs are of order  $N=2$ , that is, they are quadratic MTOs, so-called QMTOs.

The QMTO,  $\mathbf{c}_{p111}^{(2)}(\mathbf{r})$ , pointing along  $[111]$  from one Si to its nearest neighbour, is shown in the  $(2\bar{1}\bar{1})$ -plane by the first contour plot. This orbital is localized and smooth, with a few 'orthogonality wiggles' at the nearest neighbour. The remaining three contour plots show major constituents of this  $p_{111}$ -QMTO: The  $p_{111}$ -kinked partial wave (KPW),  $\mathbf{f}_{p111}^{(e)}(\mathbf{r})$ , at the central site and at the three energies  $\mathbf{e}_0, \mathbf{e}_1$ , and  $\mathbf{e}_2$ . In figure 2 we show this  $p_{111}$ -QMTO, together with the  $p_{111}$ -KPW at the three energies, along the line connecting the two nearest neighbours and proceeding into the back-bond.

In general, the members (labelled by  $R'L'$ ) of the NMTO basis set for the energy mesh  $\mathbf{e}_0, \dots, \mathbf{e}_N$  are superpositions

$$\mathbf{c}_{R'L'}^{(N)}(\mathbf{r}) = \sum_{n=0}^N \sum_{RL \in A} \mathbf{f}_{RL}(\mathbf{e}_n, \mathbf{r}) L_{nRL, R'L'}^{(N)}, \quad (1)$$

of the kinked partial waves,  $\mathbf{f}_{RL}(\mathbf{e}, \mathbf{r})$  at the  $N+1$  points (labelled by  $n$ ) of the energy mesh. In the present case, the  $L$ -summation is over the nine  $s$ -,  $p$ -, and  $d$ -KPWs, and the  $R$ -summation is over all Si sites. Due to the localized nature of the KPWs illustrated in the figures, the latter summation is limited to the neighbours. The  $RL$ -values for which we have MTOs in the basis set, we label active (A) or low. Expression (1) is the energy-quantized form of Lagrange interpolation,

$$\mathbf{c}^{(N)}(\mathbf{e}) \approx \sum_{n=0}^N \mathbf{f}(\mathbf{e}_n) l_n^{(N)}(\mathbf{e}), \quad l_n^{(N)}(\mathbf{e}) \equiv \prod_{m=0, \neq n}^N \frac{\mathbf{e} - \mathbf{e}_m}{\mathbf{e}_n - \mathbf{e}_m},$$

of a function of energy,  $\mathbf{f}(\mathbf{e})$  by an  $N$ th-degree polynomial,  $\mathbf{c}^{(N)}(\mathbf{e})$ : The  $N$ th-degree polynomial,  $l_n^{(N)}(\mathbf{e})$ , is substituted by a matrix with elements,  $L_{nRL, R'L'}^{(N)}$ , the function of energy,  $\mathbf{f}(\mathbf{e})$ , by a Hilbert space with axes,  $\mathbf{f}_{RL}(\mathbf{e}, \mathbf{r})$ , and the interpolating polynomial,  $\mathbf{c}^{(N)}(\mathbf{e})$  by a Hilbert space with axes,  $\mathbf{c}_{R'L'}^{(N)}(\mathbf{r})$ .

As illustrated in figures 1 and 2, a kinked partial wave is basically a partial wave with a tail joined continuously to it with a kink at a central, so-called hard sphere of radius  $a_R$ . This kink is seen most clearly for the lowest energy,  $\mathbf{e}_0$ . As usual, the partial wave is  $\mathbf{j}_{RL}(\mathbf{e}, r_R) Y_L(\hat{\mathbf{r}}_R)$ , where the function of energy is the regular solution of the radial Schrödinger equation,

$$- [r \mathbf{j}_{RL}(\mathbf{e}, r)]'' = [\mathbf{e} - v_R(r) - l(l+1)/r^2] r \mathbf{j}_{RL}(\mathbf{e}, r), \quad (2)$$

for the potential-well,  $v_R(r)$ . The tail of the kinked partial wave is a so-called screened spherical wave,  $\mathbf{y}_{RL}(\mathbf{e}, \mathbf{r})$ , which is essentially the solution with energy  $\mathbf{e}$  of the wave equation in the interstitial between the hard

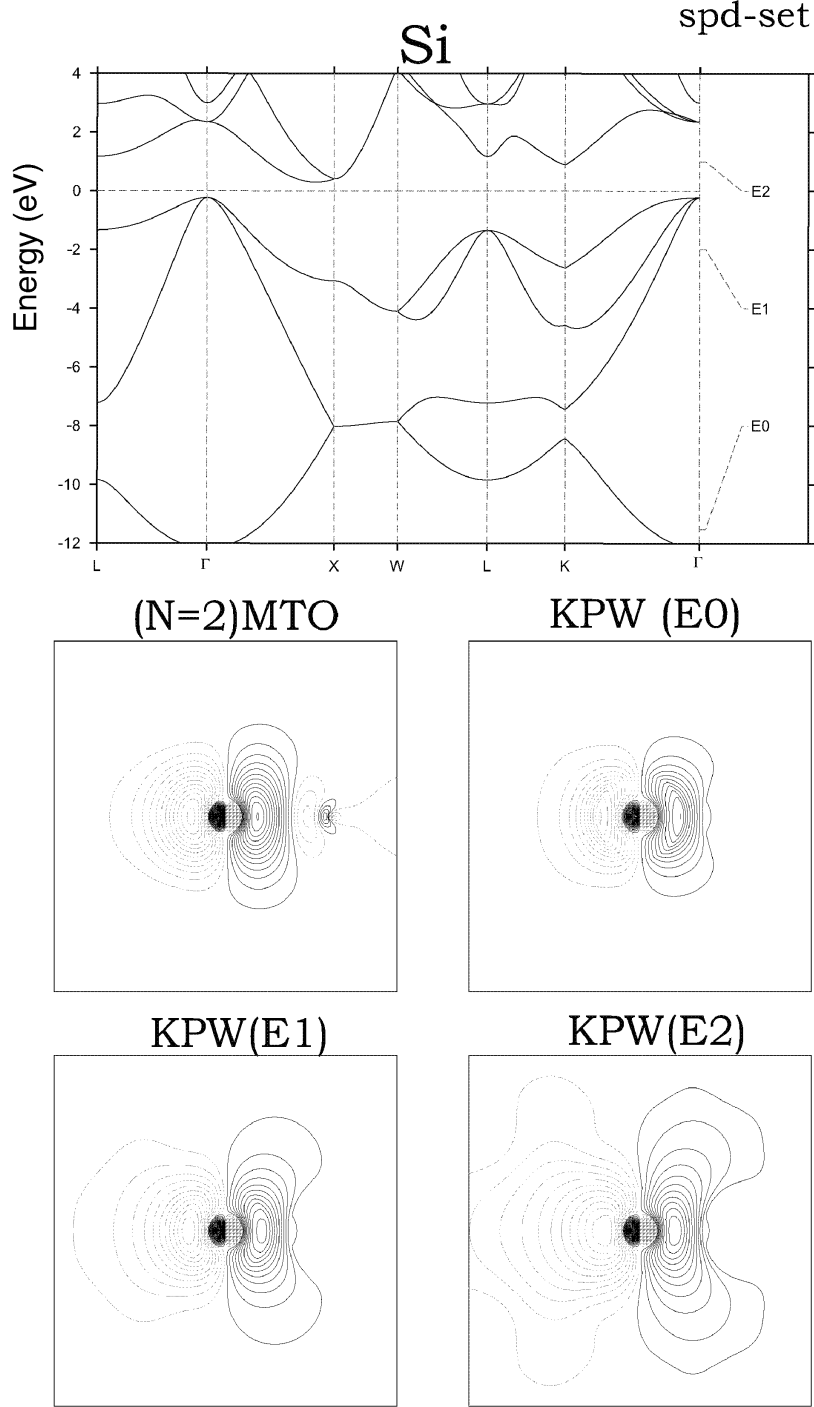


**Figure 1.** Band structure of Si calculated with the Si *spd*-QMTO basis set corresponding to the energy mesh shown on the right-hand side (solid lines). The contour plots show the Si *p* orbital pointing in the [111]-direction between two nearest neighbours in the  $(2\bar{1}1)$ -plane. Shown are the kinked partial waves (KPWs) at the three energies and the QMTO. The KPWs are normalized to 1 times a cubic harmonics, at the central hard sphere. The contours are the same in all plots.

spheres,  $-\Delta\mathbf{y}(\mathbf{e}, \mathbf{r}) = \mathbf{e}\mathbf{y}(\mathbf{e}, \mathbf{r})$ , with the boundary condition that, independent of the energy,  $\mathbf{y}_{\mathbf{r}L}(\mathbf{e}, \mathbf{r})$  go to  $Y_L(\hat{\mathbf{r}}_R)$  at the central hard sphere, and to zero (with a kink) at all other hard spheres. It is this latter confine-

ment, easily recognized in the plots, particularly at the highest energy  $\mathcal{E}_2$ , which makes the screened spherical waves, the KPWs, and the MTOs localized when the energy is not too high. At the same time, it makes the

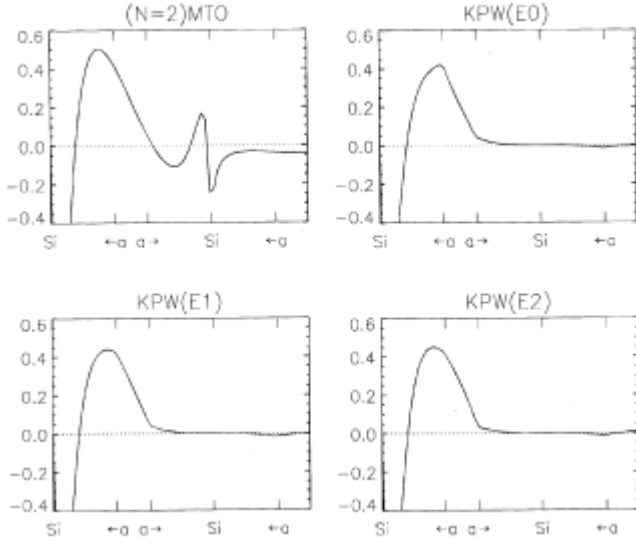


**Figure 2.** Si  $p_{111}$ -KPW for the Si  $spd$ -set plotted along the [111]-line connecting nearest neighbours. The  $a$ s indicate the hard spheres at the central and the nearest-neighbour sites. The generating MT-potential had no repulsive potential wells at interstitial sites ( $E$ ), but only large Si-centred wells with  $s = 1.7a$ .

KPW have pure  $L$ -character merely at its central sphere, because outside, it is influenced by the hard spheres centred at the neighbours. The default value of the hard-sphere radii,  $a_R$ , is 90% of the appropriate covalent, atomic, or ionic radius. The kinked partial wave thus has a kink, not only at its own, but also at the neighbouring hard spheres, inside which it essentially vanishes. ‘Essentially’ because the above-mentioned boundary condition only applies to the active components of the spherical-harmonics expansions of the screened spherical wave on the hard spheres. For the remaining components, in the present case the Si  $f$ - and higher components, as well as all components on empty ( $E$ ) spheres, the screened spherical wave equals the corresponding partial-wave solution of Schrödinger’s equation throughout the MT-sphere. The small bump seen in figure 1 in the lowest KPW contour along the [111]-direction is mainly caused by the  $f$ -character on the nearest neighbour, and so is the finite amplitude seen in figure 2 inside the nearest hard sphere.

### 3. Computational steps

The radial Schrödinger (Dirac) equation (2) is integrated numerically from  $r=0$  to  $s_R$ . This yields the radial functions,  $\mathbf{j}_{Rl}(\mathbf{e}, r)$ , and their phase shifts,  $\mathbf{h}_{Rl}(\mathbf{e})$ , each of which are obtained by matching the logarithmic derivative of  $\mathbf{j}_{Rl}(\mathbf{e}, r)$  at  $r = s_R$  to that of

$$\mathbf{j}_{Rl}^0(\mathbf{e}, r) \propto j_l(\mathbf{k}r) - \tanh \mathbf{h}_{Rl}(\mathbf{e}) n_l(\mathbf{k}r). \quad (3)$$

The radial integration must be performed for each potential well and for each  $l$ , increasing until all further phase shifts vanish due to dominance of the centrifugal term in (2).

The screened spherical waves are specified by a Hermitian structure matrix, whose element  $B_{R'L',RL}(\mathbf{e})$  is essentially the radial logarithmic derivative of the  $L'$ -component in the spherical-harmonics expansion at the hard sphere at site  $R'$  of the screened spherical wave  $\mathbf{y}_{RL}(\mathbf{e}, \mathbf{r})$ . What is known analytically, is the element

$$B_{R'L',RL}^0(\mathbf{e}) \equiv \sum_{l''} 4\mathbf{p}^{-l+l''-l''} C_{LL'l''} \mathbf{k} a_{l''}(\mathbf{k}|\mathbf{R}-\mathbf{R}'|) Y_{L''}^*(\widehat{\mathbf{R}-\mathbf{R}'}),$$

of the bare KKR structure matrix, which specifies how the spherical wave  $n_l(\mathbf{k}_R) Y_L(\hat{r}_R)$ , at site  $R$  is expanded around another site  $R'$  in regular spherical waves,  $j_{l'}(\mathbf{k}_{R'}) Y_{L'}(\hat{r}_{R'})$ . Here  $\mathbf{k} \equiv \mathbf{e}$  and the on-site terms of the bare structure matrix are defined to vanish. Screening of the structure matrix,

$$[B(\mathbf{e})^{-1}]_{RL,R'L'} \equiv [B^0(\mathbf{e})^{-1}]_{RL,R'L'} + \mathbf{k}^{-1} \tan \mathbf{a}_{RL}(\mathbf{e}) \mathbf{d}_{RR'} \mathbf{d}_{LL'},$$

requires inversion of the matrix  $B_{RL,R'L'}^0(\mathbf{e}) + \mathbf{k} \cot \mathbf{a}_{RL}(\mathbf{e}) \mathbf{d}_{R'} \mathbf{d}_{L'}$ . This can be done by fixing  $R$  and limiting  $R'$  to the 10–50 nearest sites.  $\mathbf{a}_{RL}(\mathbf{e})$  are the hard-sphere phase shifts for the active channels,

$$\tan \mathbf{a}_{RL}(\mathbf{e}) \equiv j_l(\mathbf{k}a_R)/n_l(\mathbf{k}a_R),$$

and, for the remaining channels,  $\mathbf{a}_{RL}(\mathbf{e})$  are the proper phase shifts,  $\mathbf{h}_{RL}(\mathbf{e})$ . The latter channels, which will not have KPWs and MTOs associated with them, are said to be downfolded. With appropriate division into active and downfolded channels, the screened structure matrix will have short spatial range and no poles in the energy-range of the occupied states.

A kinked partial wave is defined as

$$\mathbf{f}_{RL}(\mathbf{e}, \mathbf{r}) = [\mathbf{j}_{Rl}(\mathbf{e}, r_R) - \mathbf{j}_{Rl}^0(\mathbf{e}, r_R)] Y_L(\hat{r}_R) + \mathbf{y}_{RL}(\mathbf{e}, \mathbf{r}), \quad (4)$$

where  $\mathbf{j}(\mathbf{e}, r)$  is the radial solution for the central well from 0 to  $s$ , and  $\mathbf{j}^0(\mathbf{e}, r)$  is the phase-shifted wave (3) proceeding smoothly inwards from  $s$  to the central  $a$ -sphere, where it is matched with a kink to the screened spherical wave  $\mathbf{y}(\mathbf{e}, \mathbf{r})$ . The kinks of the KPW set are then given by the kink matrix,

$$K_{RL,R'L'}(\mathbf{e}) \equiv \frac{B_{RL,R'L'}(\mathbf{e}) + \mathbf{k} \cot \mathbf{h}_{RL}^a(\mathbf{e}) \mathbf{d}_{RR'} \mathbf{d}_{LL'}}{-\mathbf{e}_{l'}(\mathbf{k}a_R) n_{l'}(\mathbf{k}a_{R'})}, \quad (5)$$

where  $\mathbf{h}_{RL}^a(\mathbf{e})$  is the phase shift with respect to the hard-sphere medium,

$$\tan \mathbf{h}_{RL}^a(\mathbf{e}) \equiv \tan \mathbf{h}_{RL}(\mathbf{e}) - \tan \mathbf{a}_{RL}(\mathbf{e}).$$

The rows and columns of the kink matrix run merely over active channels. In the formalism above, we have for sim-

plicity used the notation of scattering theory, which is analytical for  $\mathbf{e} > 0$  and for  $\mathbf{e} < 0$ . Screened scattering theory with the normalization (5) is however analytical in a region of interest around  $\mathbf{e} = 0$ .

Finally, the Lagrange matrix which gives the MTO set (1) in terms of the KPW set (4), is given solely in terms of the values of the Green matrix,  $G(\mathbf{e}) \equiv K(\mathbf{e})^{-1}$ , on the energy mesh  $\mathbf{e} = \mathbf{e}_0, \mathbf{e}_1, \dots, \mathbf{e}_N$ . The Hamiltonian and overlap matrices in the MTO representation are given in terms of the same values of the Green matrix, plus the values of its first energy derivative,  $\dot{G}(\mathbf{e})$ .

#### 4. Further downfoldings

In the valence and lowest conduction bands of Si, there are only  $s$ - and  $p$ -, but no  $d$ -electrons. To describe these

bands, we should therefore be able to use a basis with only Si  $s$ - and  $p$ -MTOs, i.e. with only 4 orbitals per atom. We thus let the Si  $s$ - and  $p$ -partial waves remain active, while the Si  $d$ -waves are now included among the passive ones, i.e. those 'folded down' into the tails of the screened-spherical waves in (4). The results for the bands and the  $p_{111}$ -QMTO are shown in figures 3 and 4. These bands are indistinguishable from those obtained with the Si  $spd$ -set, on the scale of the figure, although between the energies of the mesh, the former bands do lie slightly above the latter. However, by making the mesh denser (increasing  $N$ ), the accuracy can be increased arbitrarily. The KPW of the  $sp$ -set is seen to have  $d$ -character on the nearest Si neighbour, and the QMTO and the KPW, particularly the one at the highest energy, are seen to be somewhat less localized than those for the  $spd$ -set.

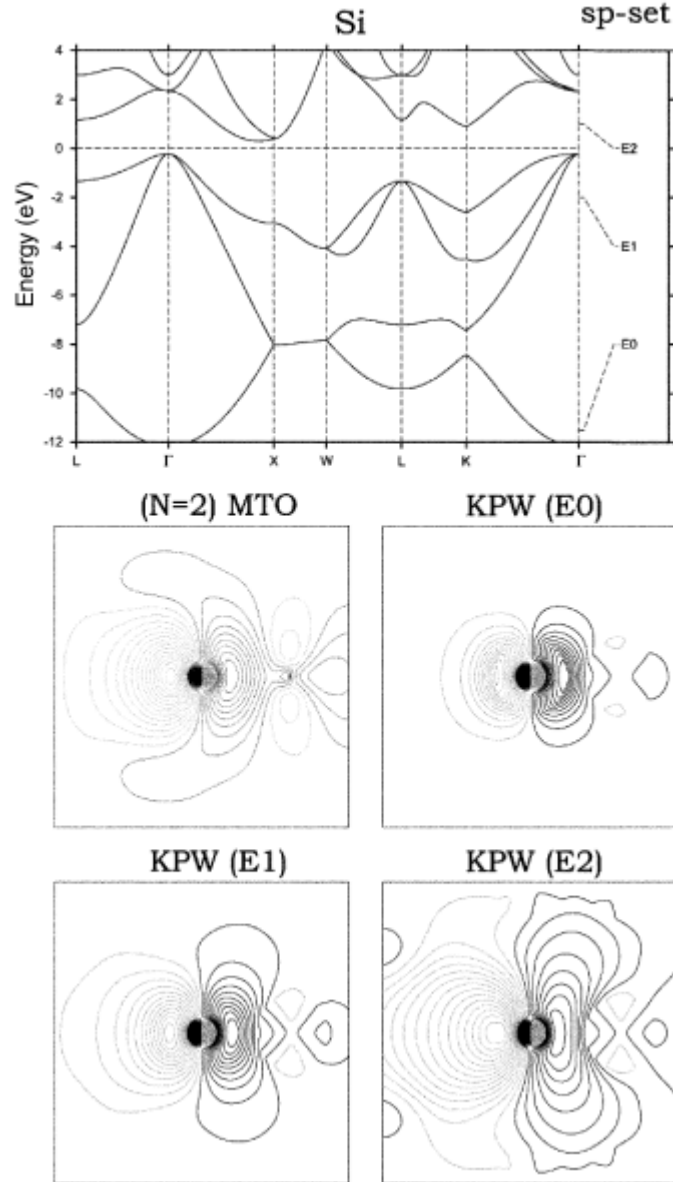


**Figure 3.** Same as figure 1, but for the Si  $sp$ -set.

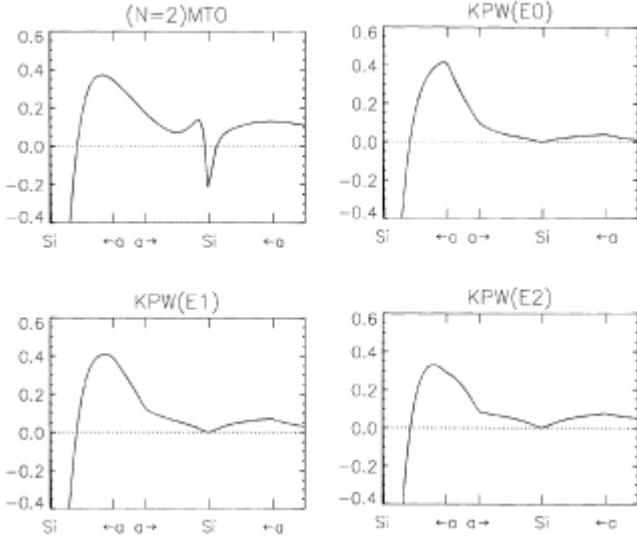


**Figure 4.** Same as figure 2, but for the Si  $sp$ -set.

It is even possible to construct an arbitrarily accurate MTO-basis which spans merely the occupied orbitals, i.e. which spans the valence band with a basis of merely 2 orbitals per atom. For tetrahedrally coordinated covalent semiconductors like Si, it is customary to take the valence-band orbitals as the bond-orbitals, which are the bonding linear combinations of directed  $sp^3$ -hybrids of orthonormal orbitals. It is, however, far simpler and more general, e.g. not limited to elemental semiconductors and tetrahedral structures, to take the valence-band orbitals as the  $s$ - and  $p$ -MTOs on every second Si atom, all partial waves on the nearest neighbours being downfolded. This corresponds to a  $\text{Si}^{4+}\text{Si}^{4-}$  ionic picture. This QMTO-set turns out to describe merely the valence band, and to do so surprisingly well considering the fact that the two silicons are treated differently, so that the degeneracy along the  $XW$ -line is, in fact, slightly broken. The error between the energy points is proportional to  $[\epsilon(\mathbf{k}) - \epsilon_0]$   $[\epsilon(\mathbf{k}) - \epsilon_1][\epsilon(\mathbf{k}) - \epsilon_2]$ , exactly as for the basis with 4 orbitals per atom shown in figure 3, because we use QMTOs in both cases, but the prefactors are larger for the smaller basis: As the number of active channels decreases, the KPWs attain longer range and stronger energy dependence. However, by making the energy mesh finer, the errors of the MTO set can be made arbitrarily small. In the bottom line of figure 5, we show the result of such a valence-band-only calculation with  $N=3$  for Ge, together with the  $p_{111}$  cubic MTO (CMTO) centred on the Ge atom to the right. The accuracy of the valence band is superb, and the MTO is seen to spill over onto the nearest-neighbour atom(s) which were chosen not to have orbitals associated with them.

Since this basis is complete for the occupied states, we may compute the density-functional ground-state properties in real space by taking traces, provided that we first

Löwdin orthonormalize the basis in real space. The sum of the one-electron energies is then computed as the trace of the Hamiltonian, i.e. as the sum of the energies of the orthonormal orbitals, and the charge density is computed as the sum of the squares of these orbitals. This is a method where the amount of computation increases merely linearly with the size of the system, a so-called order- $\bar{A}$  method. Here,  $\bar{A}$  refers to the number of atoms in the system and not to the order  $N$  of the MTOs. This NMTO method, which generates the complete basis for the occupied states *a priori*, should be superior to current order- $\bar{A}$  methods, which either use inaccurate empirical tight-binding models or project onto the occupied states during the course of a large-basis-set calculation.

In order to demonstrate in further detail that our method works, we consider Si in the diamond structure for which the valence-band Wannier functions can be taken as bond orbitals. First, we orthonormalize our symmetry-breaking  $\text{Si}^{4+}$  Si  $s$ ,  $p_x$ ,  $p_y$ ,  $p_z$  QMTO set. The resulting Si  $s$  and Si  $p_x$  orbitals are shown in the (110)-plane in figures 6 and 7. These orthogonalized orbitals are seen to remain fairly localized. Then, we transform to the four congruent  $sp^3$ -hybrids centred nominally on every second Si atom. As figure 8 shows, such an  $sp^3$ -hybrid is, in fact, the bond orbital. Hence, folding all partial waves of the atoms chosen not to carry orbitals, into the tail of the  $sp^3$ -directed orbital on one of the other Si atoms, has made that orbital look like a bond orbital. The reason why the figure does not show exact symmetry between the two sites is caused by our use of an energy mesh with only 3 points in the valence band. Making the energy mesh finer will generate the exact symmetry.

Now, Sn is metal because the bonding and antibonding bands overlap. This should, however, not prevent our method from working for the occupied states only, because NMTOs are energy selective. Since the orbitals will be shaped in such a way that the basis set solves Schrödinger's equation exactly for the energies on the mesh, we may merely have to choose several energy points in the region of band overlap below the Fermi level and, of course, no energy points above. Remember that our ionic prescription does not make use of the fact that the Wannier functions for the valence and conduction bands are respectively bonding and antibonding.

Since the ionic Si Si( $sp$ ) set gives the occupied states in diamond-structured Si with arbitrary accuracy, the same procedure with the  $sp$ -orbitals placed exclusively on the anion, and the  $d$ -orbitals on the cation, will of course work for any IV-IV, III-V, II-VI, and I-VII semiconductor and insulator. CuBr, for instance, would be thought of as an ionic compound  $\text{Cu}^+\text{Br}^-$  with the closed-shell configuration  $\text{Cu}3d^{10}\text{Br}4s^24p^6$ , and the basis should therefore have the  $d$ -MTOs on the Cu atoms and the  $s$  and  $p$ -MTOs on the Br atoms. This is illustrated in the upper line of figure 5. Being a single-site prescription, this works for CuBr in any structure. What we have

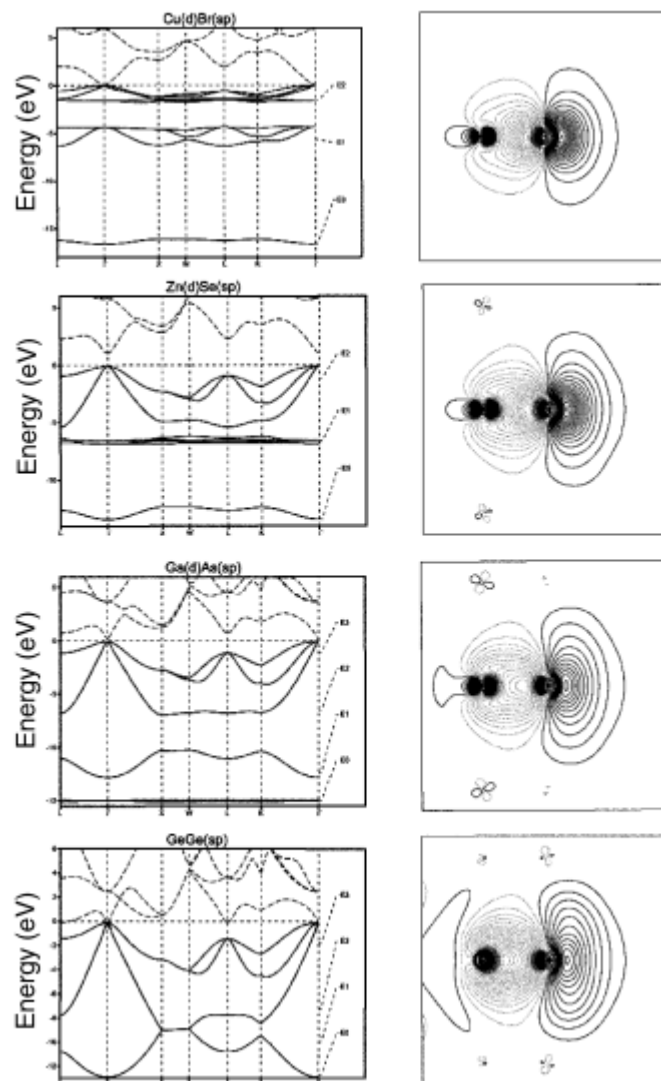


**Figure 5.** Valence bands (solid lines) of the series CuBr–Ge, calculated with the ionic basis sets where the  $sp$ -MTOs are on the anion and, except for Ge, the  $d$ -MTOs are on the cation. The exact bands are given by dashed lines. The contour plots show the  $p_{111}$ -MTO on the anion (the atom to the right). The ionicity decreases and the covalency increases from the top to the bottom.

seen is thus, that the MTO basis can be designed *a priori* to span the Hilbert space of the occupied states only. That is, there is one, and only one, such MTO per electron. To specify such a set, one would, in order to get the electron-count right, put the orbitals where the electrons are thought to be, and leave it to the method to shape the tails of these orbitals in such a way that the basis solves Schrödinger's equation exactly for occupied states of the given static mean-field (e.g. LDA) potential. Such ionic MTO basis sets, which 'automatically' span the occupied—and no further—states of any band insulator, could make density-functional molecular-dynamics calculations highly efficient for such systems.

How could one imagine to treat a chemical reaction like:  $2\text{H}_2\text{O} \rightarrow 2\text{H}_2 + \text{O}_2$  with MTO bases of occupied states only? For water, it is natural to use the ionic

description  $\text{H}_2^+\text{O}^{--}$ , according to which the orbital configuration is  $\text{O } p^6$ , i.e. one would put the  $p$  orbitals on oxygen and fold down all partial waves centred on the hydrogens. In principle, one might stick to this configuration throughout the reaction, because it keeps the electron-count right. However, the oxygen-centred orbitals would eventually look strange and have long range, because they would have to separate off pieces of wave functions sitting on the hydrogens. Such oxygen orbitals might be more time-consuming to generate. At some stage in the reaction, it might therefore be appropriate to switch to configurations such as  $\text{H}s^\uparrow\text{H}s^\downarrow$ , or  $\text{H } \text{H}s^2$  for the hydrogen molecule; this is analogous to our treatment of the occupied states in tetrahedrally coordinated Si. For  $\text{O}_2$  with the open-shell molecular configuration  $pp\bar{s}^2 pp\bar{p}^4$ , we might use an 'ionic' configuration like:

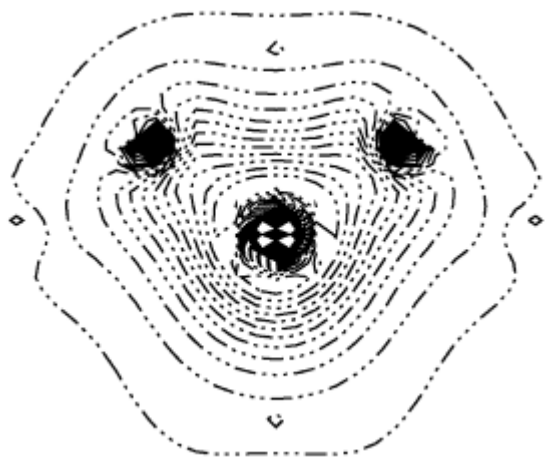


**Figure 6.** Contour plot in the  $(1\bar{1}0)$ -plane of the orthogonalized  $s$ -QMTO on the central Si atom. All partial waves on the nearest neighbours (and their lattice translations) were down-folded.

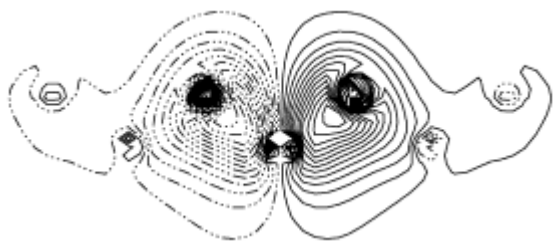


**Figure 7.** Same as figure 6, but for the  $p_x$ -QMTO.

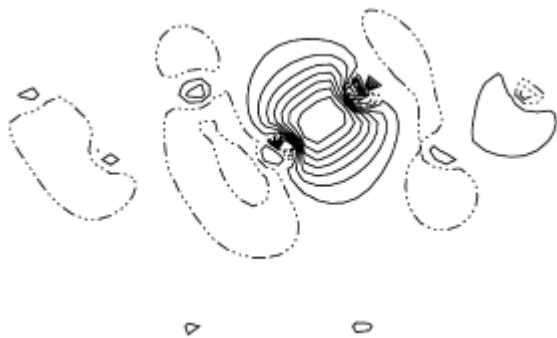


**Figure 8.** Same as figure 6, but for the  $sp^3$ -hybrid. For increasing  $N$ , this orbital converges to the bond orbital.

$O(z\uparrow x\uparrow y\uparrow)$   $O(z\downarrow x\uparrow y\uparrow\downarrow)$  with  $z$  referring to the local  $z$ -direction of the molecule.

This example immediately leads to a treatment of open-shell systems by means of spin and possibly orbital polarizations. We have seen that the 3rd-generation MTO method offers the possibility of designing single-electron bases of atom-centred localized orbitals, which span the wave functions in a given energy region of a given mean-field potential. These orbitals can even be symmetry-breaking, as in the case of diamond, Si, Ge, and Sn, without the generating mean field having to be so. These

orbitals thus seem to have great potential in the design of many-electron wave functions which describe correlated electron systems in a realistic way.

## 5. Conclusion

We have solved the long-standing problem of deriving energy-independent, short-ranged orbitals from scattering theory (Hubbard 1967). The present formalism contains exactly the right ‘physics and chemistry,’ we feel. This should give the computational method great speed and accuracy, and make it a vehicle for discovery and understanding.

## References

- Andersen O K and Jepsen O 1984 *Phys. Rev. Lett.* **53** 2571  
 Andersen O K and Saha-Dasgupta T 2000 *Phys. Rev.* **B62** R16 219  
 Andersen O K, Postnikov A V and Savrasov S Yu 1992 *Applications of multiple scattering theory to materials science, Mat. Res. Soc. Symp. Proc.* (eds) W H Butler, P H Dederichs, A Gonis and R L Weaver (Pittsburgh: Materials Research Society) Vol. **253**, pp 37–70  
 Andersen O K, Jepsen O and Krier G 1994 *Lectures on methods of electronic structure calculations* (eds) V Kumar, O K Andersen, and A Mookerjee (Singapore: World Scientific Publishing Co) pp 63–124  
 Andersen O K, Arcangeli C, Tank R W, Saha-Dasgupta T, Krier G, Jepsen O and Dasgupta I 1998 *Tight-binding approach to computational materials science, Mat. Res. Soc. Symp. Proc.* (eds) L Colombo, A Gonis and P Turchi (Pittsburgh: Materials Research Society) Vol. **491**, pp 3–34  
 Andersen O K, Saha-Dasgupta T, Tank R W, Arcangeli C, Jepsen O and Krier G 2000 *Electronic structure and physical properties of solids. The uses of the LMTO method* (ed.) H Dreyse (New York: Springer Lecture Notes in Physics) pp 3–84  
 Arcangeli C and Andersen O K, to be published  
 Dasgupta I *et al*, to be published  
 Dasgupta I, Saha-Dasgupta T, Andersen O K, Pavarini E and Jepsen O, to be published  
 Hubbard J 1967 *Proc. Phys. Soc. London* **91** 921 and references therein  
 Kohn W and Rostoker J 1954 *Phys. Rev.* **94** 111  
 Korotin M A, Anisimov V I, Saha-Dasgupta T and Dasgupta I 2000 *J. Phys. Cond. Matter* **12** 113  
 Korringa J 1947 *Physica* **13** 392  
 Müller T F A, Anisimov V, Rice T M, Dasgupta I and Saha-Dasgupta T 1998 *Phys. Rev.* **B57** R12655  
 Pavarini E, Dasgupta I, Saha-Dasgupta T, Jepsen O and Andersen O K 2001 *Phys. Rev. Lett.* **87** 047003  
 Sarma D D, Mahadevan P, Saha-Dasgupta T, Ray S and Kumar A 2000 *Phys. Rev. Lett.* **85** 2549  
 Savrasov D and Andersen O K, to be published  
 Tank R W and Arcangeli C 2000 *Phys. Status Solidi* (b)**217** 89  
 Valenti R, Saha-Dasgupta T, Alvarez J V, Pozgajcic K and Gros C 2001 *Phys. Rev. Lett.* **86** 5381  
 Zeller R, Dederichs P H, Ujfalussy B, Szunyogh L and Weinberger P 1995 *Phys. Rev.* **B52** 8807